《原　著》

EVALUATION OF SCINTILLATION CAMERA PERFORMANCE FOR LOW-CONTRAST OBJECTS

Ken UEDA* and Kenji ISHIMATSU**

ABSTRACT Scintillation camera imaging performance for low-contrast ^{99m}Tc or ^{131}I distribution patterns is investigated theoretically. The present method is based on an evaluation of "scinti-photo resolution", which is a complex function of the intrinsic resolution and sensitivity of the camera, collimator performance, imaging time, radioactivity and object pattern contrast. A "characteristic curve" is defined as the relation between distance to be resolved and the minimum product of radioactivity and imaging time. A mathematical expression of the curve is derived from an expansion of the semi-empirical expression which has been confirmed experimentally for bar-phantom images. Typical characteristic curves for recent high-resolution systems are represented.

An optimum collimator selection method is described by comparing characteristic curves for different collimators. Next, the effects of intrinsic spatial resolution change and detection sensitivity change on characteristic curves are examined. The former and latter are determinant factors for ^{99m}Tc and ^{131}I imaging, respectively. Comparative evaluation among different systems appears to be basically unaffected by the object contrast.

"Scinti-photo resolution", defined as the resolution of scinti-photos, for bar-phantoms was previously investigated theoretically and experimentally in relation to system resolution and sensitivity[1]. The relation between bar width (x) and the minimum product (aT) of radioactivity density (a) and imaging time (T) for recognizing bars in an image was given theoretically. This relation, which is the "characteristic curve" for the system, was shown to be suitable for evaluating system performance. The "characteristic curves" obtained experimentally for ^{99m}Tc (140 keV) gamma-rays agreed with the theoretical results within the experimental error limits.

In this paper, system performance for low-contrast radioactivity distribution patterns is invenstigated according to a similar theoretical process. First, a mathematical expression of the "characteristic curves" expanded for low-contrast object is derived. Next, an optimum-collimator selection method is described based on comparison of different characteristic curves, when the scinti-photo resolution required or radioactivity density and imaging time are given beforehand. Then, effects of both the intrinsic resolution of scintillation cameras and detection efficiency of scintillation crystals on the characteristic curves are evaluated. These discussions are entirely conducted for ^{99m}Tc (140 keV) gamma-rays. Finally, system performance for high-energy ^{131}I(364ke V) gamma-rays is evaluated using a similar method, and characteristic features of high-energy gamma-rays are discussed.

* Hitachi Central Research Loboratory, Hitachi Ltd., Tokyo
** Hitachi Medical Corporation, Tokyo
受付：53年5月4日
最終稿受付：54年11月22日
別刷請求先：国分寺市東恋ケ窪1-280 (〒185)
株式会社日立製作所中央研究所
植　田　　健

The "Characteristic Curves" for Low-contrast Object

A one-dimensional model for a low-contrast object pattern is shown in Fig. 1. A one-dimensional model of the corresponding image is also shown. As a measure of radioactivity density contrast, the ratio of defect depth to peak concentration, $1/b$, is employed throughout the analysis. Object contrast, C, in general use, is:

$$C = \frac{1}{2 \cdot b - 1} \tag{1}$$

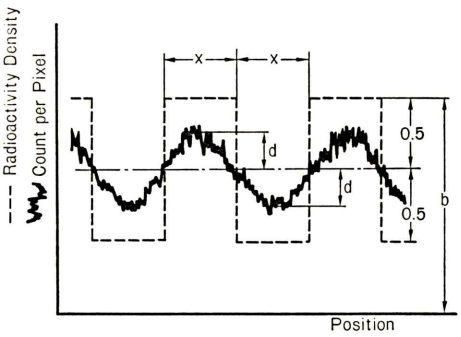

Fig. 1 One-dimensional models for object patterns and corresponding images. Broken line represents low-contrast object. Solid line represents corresponding scintigram profiles including Poisson noise.

Regarding the image models, the average count, B, per picture element (pixel) in the hottest region, and the difference, p, between the counts in the hottest and coldest regions are expressed as follows:

$$B = \frac{b-0.5+d}{b-0.5} \cdot n_{av} \cdot S_e \tag{2}$$

$$p = \frac{2 \cdot d}{b-0.5} \cdot n_{av} \cdot S_e \tag{3}$$

where,

n_{av} : the average information density, i.e. the average count per unit area at the detector surface,

S_e: the area of a virtual pixel[1], which is the resolvable area by human eyes, and

d: defined as in Fig. 1, related to the contrast of images.

The line spread function of the system is assumed to be a normal Gaussian distribution function. Then, the system spatial resolution is represented in terms of the standard deviation, s_t, or full width at half maximum (FWHM), $R_t(=2.35 \cdot s_t)$.

Here, the object pattern, $h(z)$, and line spread function, $q(z)$, are expressed in mathematical form as:

$$h(z) = b-1+\sum_{n=-\infty}^{\infty} \mathrm{rect}\left(\frac{z-2 \cdot x \cdot n}{x}\right) \tag{4}$$

$$q(z) = \frac{1}{\sqrt{2\pi} \cdot s_t} \cdot \exp\left(-\frac{z^2}{2 \cdot s_t^2}\right) \tag{5}$$

where, x is defined in Fig. 1, and:

$$\mathrm{rect}\left(\frac{z}{x}\right) \equiv \begin{cases} 1, & \text{for } |z| < x/2 \\ 0, & \text{for } |z| > x/2 \end{cases} \tag{6}$$

Consequently, the image pattern, $I(z)$, is obtained from the convolution integral of $h(z)$ and $q(z)$ as:

$$I(z) = \int_{-\infty}^{+\infty} h(t) \cdot q(z-t)\, dt \tag{7}$$

$$= b-1+\frac{1}{\sqrt{2\pi} \cdot s_t} \sum_{n=-\infty}^{\infty} \cdot \int_{2xn-x/2}^{2xn+x/2} \exp\left(-\frac{(z-t)^2}{2 \cdot s_t^2}\right) dt\,. \tag{8}$$

The valued of d is obtained from:

$$d = \frac{I(0)-I(x)}{2} \tag{9}$$

It should be noted that d is a function of only x/s_t.

With regard to the critical limit of human eyes for recognizing bars in a bar-phantom scintigram, originally including Poisson noise, the following semi-empirical formula[2] is applied:

$$\sqrt{B}/p = 1 \tag{10}$$

The area of a virtual pixel, S_e, is assumed to be:

$$S_e = k \cdot x^2 \tag{11}$$

where k is a constant. This assumption is based on the previous experimental results[1]. The value of k is considered a kind of correction factor for eq. (10), and is affected by the criteria for classification by human eye measurement into the following three classes: resolved, critical, and unresolved. The value, $k=0.172$, previously determined experimentally[1] is applied here.

The combination of eqs. (2), (3), (10) and (11) leads to:

$$n_{av} \cdot s_t^2 = \frac{(b-0.5+d) \cdot (b-0.5)}{k \cdot (2d)^2 \cdot (x/s_t)^2} \equiv F(x/s_t, 1/b) \tag{12}$$

The term, $n_{av} \cdot s_t^2$, is a function of $1/b$ and x/s_t, since d is a function of x/s_t.

Gamma-ray counting efficiency is expressed as:

$$\frac{n_{av}}{aT} = 2.22 \cdot 10^9 \cdot f \cdot e \cdot g \cdot w \tag{13}$$

where,

a: average radioactivity density in the object pattern ($\mathrm{mCi \cdot cm^{-2}}$),

T: imaging time (min),
f: number of emitted gamma-rays per disintegration,
e: photopeak efficiency of the scintillation crystal,
g: geometrical efficiency of the collimator, and
w: efficiency of the pulse-height selector, i.e. the ratio of the number of pulses impinging in the pulse-height selector window to that involved in the photopeak.

The minimum product of radioactivity density and imaging time (critical aT) for resolving distance x is determined by the following equation, derived from eqs. (12) and (13):

$$aT = 4 \cdot 51 \cdot 10^{-10} \cdot \frac{F(x/s_t, 1/b)}{f \cdot e \cdot g \cdot w \cdot {s_t}^2} \qquad (14)$$

The characteristic curves are calculated using this equation.

An expression for high-contrast objects is obtained by substituting $1/b = 1.0$ in eq. (14). When the expression thus obtained is compared to the expression for bar-phantoms, (eq. (9) in Reference (1)), the corresponding aT for an equivalent x is equal to half of the value for bar phantoms. This is because the high-contrast distribution requires half the radioactivity of a model for flood source and bar-phantom combination, since the efficiency of bar-phantoms is 1/2.

The value of s_t in eq. (14) is determined from:

$$s_t = 0.4247 \cdot (R_i^2 + R_c^2)^{1/2} \qquad (15)$$

Where R_i is the intrinsic spatial resolution of the scintillation camera in terms of FWHM, and R_c is the collimator spatial resolution in terms of FWHM at the object position.

With regard to geometrical efficiency, g, in eq. (14), maximum collimator efficiency, g_{max}, exists for collimators having a certain R_c, that is:

$$g_{max} = 0.3294 \cdot 10^{-5} \cdot {R_c}^2 \qquad (16)$$

for ^{99m}Tc (140keV) gamma-rays, when R_c is represented in "mm"[1]. The g_{max} values are realized approximately with well-designed collimators.

Typical characteristic curves for various $1/b$ values are presented in Fig. 2, for a ^{99m}Tc distribution pattern 100 mm from the colimator surface. The parameter conditions in eq. (14) are: $f = 1.0$, $e = 0.707$ for a 9 mm thick NaI (Tl) crystal, $g = g_{max}$, $R_i = 3.53$ (mm), and $R_c = 5.0$ (mm). Here, photopeak selection efficiency of the pulse-height selector is assumed to be 1.0.

It is obvious in Fig. 2, that as object contrast decreases, the critical aT for recognizing a certain x increases, and the resolving distance increases for a certain aT value.

Deterioration in resolving distance resulting from the decrease in object contrast, for various aT valueds is shown in Fig. 3. The figure is obtained from a transformation of Fig. 2. It is shown that the deterioration increases to a certain degree as aT decreases.

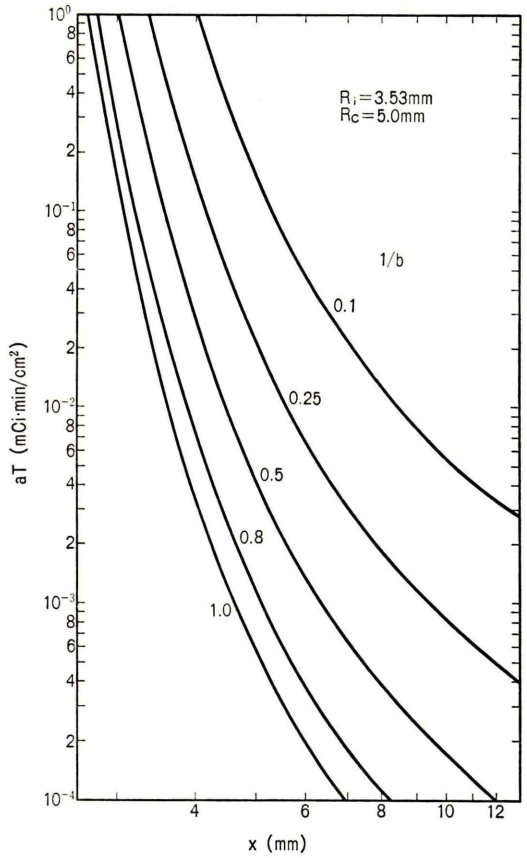

Fig. 2 Typical "characteristic curves" for various 1/b's. High-resolution system and ^{99m}Tc distribution patterns are assumed. Detail conditions are presented in the text.

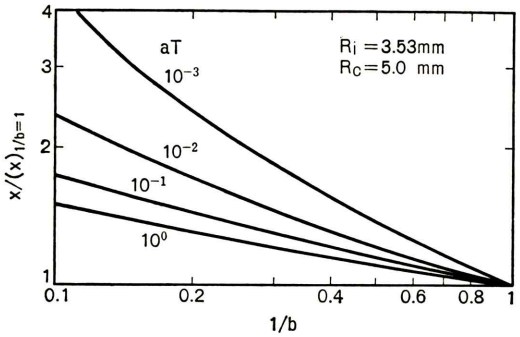

Fig. 3 Examples of relative resolving distance versus 1/b for various aT values.

The increase in the critical aT in relation to the decrease in object contrast is depicted in Fig. 4. This is obtained from the following expression which is derived from eqs. (12) and (14):

$$\frac{aT}{(aT)_{1/b=1.0}} = \frac{2(b-0.5)(b-1)}{0.5+d} + 2(b-0.5) \quad (17)$$

Since d is a function of x/s_t, $aT/(aT)_{1/b=1.0}$ is a function of only $1/b$ and x/s_t. It should be noted that this figure is applicable to any s_t or gamma-ray energy condition, since the distance to be resolved is normalized with x/s_t. The figure shows that the critical aT increases remarkably as object contrast decreases. The effect of x/s_t variations on $aT/(aT)_{1/b=1.0}$ is relatively small.

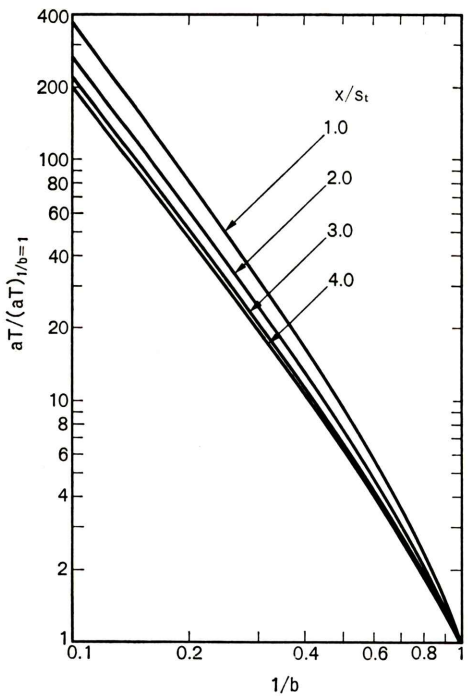

Fig. 4 Relative critical aT versus 1/b for various relative resolution distances. This relation is independent of s_t or gamma-ray energy conditions.

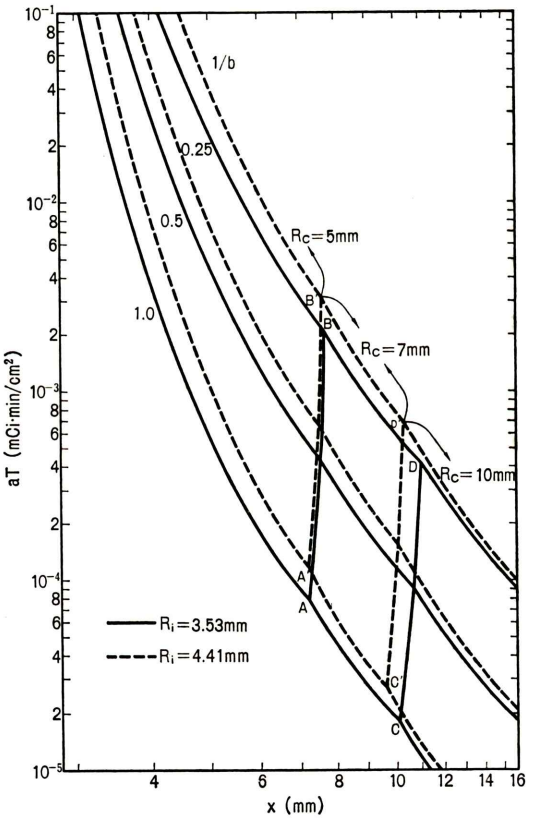

Fig. 5 Selection of the optimum collimator for ^{99m}Tc. Characteristic curves for three different collimators are shown in the region where they are optimum. Lines A-B, A′-B′, C-D and C′-D′ show border lines determining optimum collimators.

Optimum Collimator Selection

When characteristic curves are obtained for various different collimators, a collimator which provides the minimum aT in a certain x region is the optimum collimator for that x region. In other words, the collimator which gives the minimum x in a certain aT region is optimum for that aT region.

The characteristic curves for $R_c=7$ and 10 (mm) were examined for various object contrast conditions, according to the same method used for $R_c=5$ (mm). Other parameter conditions are the same as those in Fig. 2, i.e. $f=1.0$, $e=0.707$, $g=g_{max}$, and $R_i=3.53$ (mm). These values represent the performance of a commercial scintillation camera system, Hitachi "GAMMA VIEW", and its standard collimators for low-energy gamma-rays[3].

Comparing characteristic curves for these three R_c's, the optimum collimators are selected according to various $1/b$ and x values. The results are shown as solid lines in Fig. 5. The broken lines in this figure show the results for a supposed system having a 25 percent larger R_i, which will be discussed in the following section.

The border lines determining optimum collimators have large inclinations in Fig. 5. Therefore, when the distance to be resolved in determined first, the optimum collimator is decided almost independent of object contrast.

The critical aT, however, increases considerably as object contrast decreases. This implies that much longer imaging time or much more radioactivity is required as object contrast decreases.

Therefore, aT, rather than x, is usually determined before imaging. From this point of view, selection of the optimum collimator is affected by both aT and $1/b$. For instance, when $aT=2.10^{-4}$ (mCi.min.cm^{-2}) is planned for beforehand, the optimum collimator for $1/b=1.0$, 0.5, and 0.25 is the collimator with $R_c=5$, 7 and 10 (mm), respectively. A map for optimum collimator selection for given aT and $1/b$ values is shown in Fig. 6.

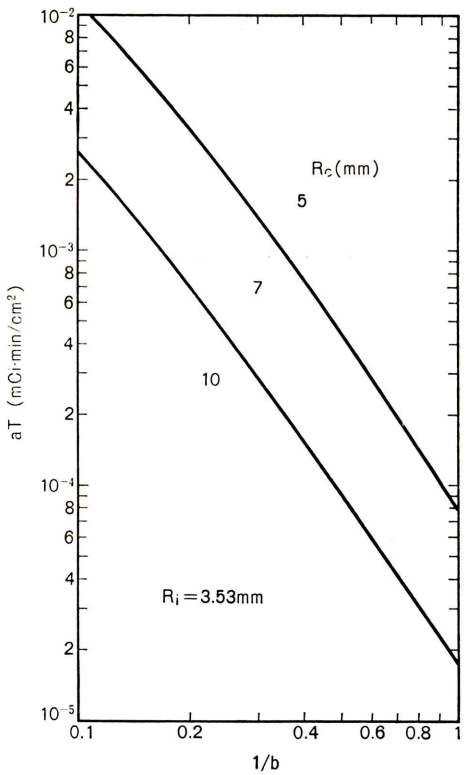

Fig. 6 Optimum collimators for ^{99m}Tc, for given aT and 1/b.

Effect of Intrinsic Spatial Resolution and Detection Sensitivity

When R_i increases, individual characteristic

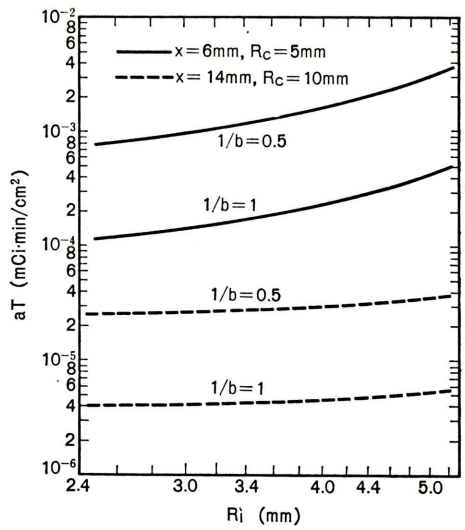

Fig. 7 Effect of R_i change on critical aT for ^{99m}Tc.

curves move to the right and remain parallel in the log log scale coordinate system shown in Fig. 5. The movement distance is a complicated function of x, s_t, and $1/b$ (see eqs. (12) and (14)). As is evident from Fig. 5, however, the movement distance is only slightly affected by the difference in $1/b$.

The critical aT is related to R_t for certain $1/b$'s, when the distance to be resolved is fixed. The results with four typical cases are shown in Fig. 7. In two cases, a considerably small distance, $x=6$ (mm), is to be resolved, and the high-resolution collimator having $R_c=5$ (mm) is applied. In the other two cases, a considerably large distance, $x=14$ (mm), is to be resolved, and the high-sensitivity collimator having $R_c=10$ (mm) is applied. It should be noted that when the curves where $1/b=1.0$ are moved parallel in upper direction, they almost agree with other curves where $1/b=0.5$.

Therefore, the effect of R_t change on critical aT is nearly unaffected by variations of $1/b$.

Meanwhile, increases or decreases in the gamma-ray detection sensitivity cause movement of the curves in Fig. 7 in the lower or upper directions, respectively. Therefore, comparison between different systems having various detection sensitivities is possible.

Scintillation crystal thickness of the system under consideration (Hitachi GAMMA VIEW) is 9 mm, while typical thickness for other commercial scintillation cameras is 12.7 mm. The crystal thickness, t, is a primary factor for determining the photopeak efficiency, e, in eq. (14). The change from $t=9$ to 12.7 (mm) increases e for ^{99m}Tc gamma-rays by 6 percent, and decreases the critical aT by the same factor.

A system which provides less or more aT for fixed x and $1/b$ values is considered to have higher or lower "imaging performance", respectively. The system having $t=12.7$ (mm) and only 5 percent larger R_t yields "imaging performance" equivalent to GAMMA VIEW, under the conditions where $x=6$ (mm) is to be resolved. The system having 15 percent larger R_t is equivalent when $x=14$ (mm) is to be resolved.

System Performance for ^{133}I

The GAMMA VIEW characteristic curves for ^{131}I are considered here. The R_t value for ^{131}I is

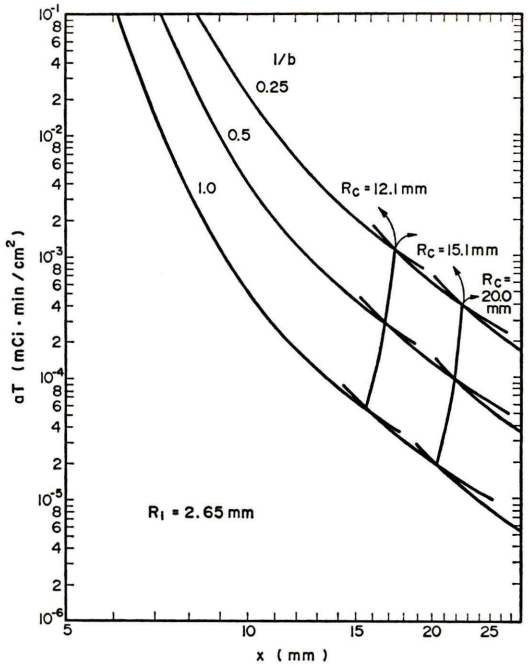

Fig. 8 Selection of the optimum collimator for ^{131}I. Lines A-B, A′-B′, C-D and C′-D′ show border lines determining optimum collimators.

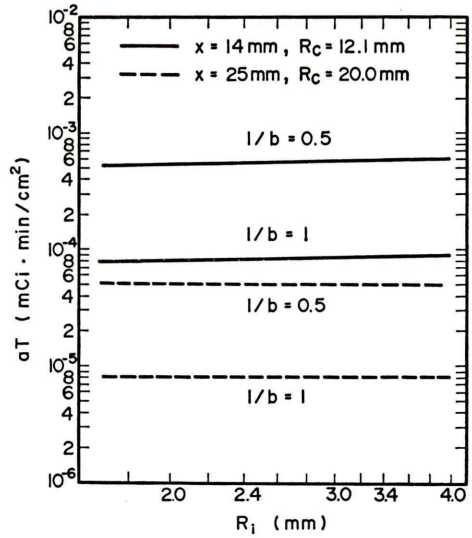

Fig. 9 Effect of R_t change on critical aT for ^{131}I.

assumed to be 2.65 (mm), although the value has not been measured. This assumption is based on the average R_t ratio of 364 to 140 keV interpolated for other scintillation cameras using delay-line principle, that is, the average ratio can be read as 3/4 from Fig. 2 in Reference (4) and Fig. 6 in Reference (5).

Three middle-energy collimators having $R_c=$ 12.1, 15.1 and 20.0 (mm) for an object 100 mm away from the collimator surface are taken into consideration. The e and f values for ^{131}I are assumed to be $f=0.82$[6], $e=0.0957$ for $t=9$ (mm), and $e=0.125$ for t=12.7 (mm).

The characteristic curves are shown in Fig. 8. Comparing this figure with Fig. 6 for ^{99m}Tc, the resolving distance for a fixed aT is about twice that for ^{99m}Tc, and the critical aT for a fixed resolving distance is much larger than ^{99m}Tc. The main reason for this is that collimators for ^{131}I have a much smaller g than for ^{99m}Tc (see eq. (10) in Reference (1)).

Typical examples of the relationship between critical aT and R_t for fixed x and $1/b$ are represented in Fig. 9. Characteristic curves for systems having $t=12.7$ (mm) lie 30 percent below the curves in Fig. 9. Consequently, a system having $t=12.7$ (mm) and as much as 85 percent larger R_t has "imaging performance" equivalent to GAMMA VIEW, under the condition where $x=14$ (mm) is to be resolved. This is not largely affected by $1/b$ variations. Thus, "imaging performance" is affected considerably by e, or t, rather than R_t.

Conclusion

The performance evaluation method for scintillation camera systems proposed previously[1] has been expanded for low-contrast ^{99m}Tc and ^{131}I distribution. The present work does not include experimental work for comparison, whereas experimental results agreed with the theoretical ones within the experimental error in the previous paper. This analysis, however, is expected to prove dependable to the same degree as the previous one, since no major new assumptions have been added.

When some biological parameters such as the depth and projected area of organs under study and isotope uptake ratio are known, an optimum collimator can be determined. Then scintigram resolution and detectable contrast can be accurately estimated.

Some unresolved correction factors remain, however, such as the effect of Compton scattering gamma-rays, the case for irregular pattern recognition, which are always incidental to practical imaging. Experimental work under practical conditions is required to clarify these areas more completely.

Acknowledgment

The authors are indebted to Dr. Katsumi Takami and Mr. Fumio Kawaguchi of Hitachi Central Research Laboratory for their valuable suggestions made during discussions.

The present work was originally presented at the 17th Annual Meeting of Japanese Society of Nuclear Medicine in November 1977.

REFERENCES

1) Ishimatsu K, Ueda K, Tanaka M, et al: Scinti-photo resolution and evaluation of scintillation camera system. Jap J Nucl Med: to be published
2) Iinuma T, Fukuhisa K: Digital simulation of radioisotope imaging (1). On the recognition of a defect in plane source by human observer. Nippon Acta Radiologica **31**: 1270–1285 1972 (In Japanese)
3) Nagasawa Y, Ishimatsu K, Tabuchi H: Development of a scintillation camera "GAMMA VIEW".: Hitachi Hyoron 59: 168–172, 1977 (In Japanese) and abstract in Hitachi Review **26**: 102, 1977
4) Nohara N, Tanaka E, Hiramoto T: High-resolution scinticamera based on delay-line time conversion. J Nucl Med **12**: 635–636, 1971
5) Tanaka E, Nohara N, Kumano N, et al.: A large-area, high-resolution scintillation camera based on delay-line time conversion. In Medical Radioisotopes scintigraphy 1972, Vol 1, Vienna, IAEA, 1973, pp 169–180
6) Lederer MC, Hollander JM, Perlman I: Table of Isotopes. 6th ed., Wiley, New York, 1967, p. 70

要　旨

低コントラスト被写体に対するシンチカメラ性能の評価

植田　健*　石松　健二**

* ㈱日立製作所中央研究所，** ㈱日立メディコ

シンチグラムの解像度に関する特性曲線（バーファントム幅と，それを見分けるに必要な RI 投与量 (a) と撮像時間 (T) との積 (aT) との関係）は，検出器およびコリメータの感度と解像度によって決定される．この特性曲線を RI 分布が低濃度差である被写体に対して理論的に検討した．^{99m}Tc および ^{131}I に対して，被写体コントラスト，シンチグラム解像度，および撮像条件 (aT) の3因子の2因子を指定したときに，検出器の解像度に応じて最適なコリメータを選択する方法を示した．最適コリメーターの選定は，被写体コントラストにはほとんど影響されないが，同一 aT 値のときのシンチグラム解像度に対するコントラストの影響は大きい．検出器の解像度および検出効率（シンチレーター厚）の変化が特性曲線に与える影響を定量化した結果，同一の解像度を得るに必要な aT 値の大きさには，^{99m}Tc では前者が，^{131}I では後者が支配的であった．

Key word: Comera performance for low-contrast